

Parameter Design for A 6.78-MHz Wireless Power Transfer System Based on Analytical Derivation of Class E Current-Driven Rectifier

Ming Liu, *Student Member, IEEE*, Minfan Fu, *Student Member, IEEE*, Chengbin Ma, *Member, IEEE*

Abstract—Magnetic resonance coupling working at megahertz (MHz) is widely considered a promising technology for the mid-range transfer of a medium amount of power. It is known that the soft-switching based Class E rectifiers are suitable for high-frequency rectification, and thus potentially improve the overall efficiency of MHz wireless power transfer (WPT) systems. This paper reports new results on optimized parameter design of a MHz WPT system based on the analytical derivation of a Class E current-driven rectifier. The input impedance of the Class E rectifier is accurately derived, for the first time, considering the on-resistance of the diode and the equivalent series resistance of the filter inductor. This derived input impedance is then used to develop and guide design procedures that determine the optimal parameters of the rectifier, coupling coils, and a Class E PA in an example 6.78-MHz WPT system. Furthermore, the efficiencies of these three components and the overall WPT system are also analytically derived for design and evaluation purposes. In the final experiments, the analytical results are found to well match the experimental results. With loosely coupled coils (mutual inductance coefficient $k=0.1327$), the experimental 6.78-MHz WPT system can achieve 84% efficiency at a power level of 20 Watts.

Index Terms—Wireless power transfer, magnetic resonance coupling, Class E rectifier, parameter design.

I. INTRODUCTION

Wireless power transfer (WPT) is now attracting considerable attention both from academia and industry largely due to the need to charge various electronic devices, e.g., cellphones, laptop computers, tablets, medical implant devices. It is desired by the end-users to access to both information and electrical power through air. For high-power applications such as charging of robots and electric vehicles, WPT provides a convenient and safe non-contacting charging, and brings new possibilities for energy and power management. The technological options for WPT (such as inductive coupling, magnetic coupling, microwave and laser radiation) have different power level, working frequency, transfer distance, size and forming factors, etc [1]–[5]. Among these technologies, the magnetic resonance coupling working at megahertz (MHz) is being widely considered a promising candidate for the mid-range transfer of a medium amount of power [5], [6]. It is because

generally a higher operating frequency (such as 6.78 and 13.56 MHz) is desirable for a more compact and lighter WPT system with a longer transfer distance. Lots of research has been done on the design and optimization of WPT systems both at component and system levels, including the improvements on coupling coils [7]–[11], power amplifier (PA) [12]–[15], and load control [16]–[18]. Meanwhile, there are few discussions on the analysis of the rectifier and its interactive relationship with other components (such as the coupling coils and PA) in a WPT system, especially when the operating frequency is at MHz. So far, most WPT systems use the hard-switching based rectifiers, e.g. the full-bridge rectifiers. In order to reduce the switching loss at MHz, the soft-switching techniques can be applied to rectifiers working at high frequencies. It is known that Class E rectifiers are one of the most promising candidates for the high-frequency rectification due to their capability of zero-voltage switching (ZVS), low voltage-slope (dv/dt) switching, zero-current switching (ZCS), and low current-slope (di/dt) switching of the rectifying element [19], [20].

The Class E rectifier was first proposed for high-frequency DC-DC converter applications in 1988 [21]. Various Class E topologies were later developed, such as voltage-driven [22], [23], current-driven [24]–[26], and full-wave ones [27]. Recently researchers have started to apply the Class E rectifiers in WPT systems. [28] discussed, for the first time, the application of the Class E rectifier in a 800-kHz WPT system. [29] presented a state-space based analysis of a Class E^2 converter, i.e., a Class E PA and a Class E rectifier, for a 200-kHz WPT systems. In [30] a Class E^2 DC-DC converter was designed and implemented for an application in 200-kHz WPT. Meanwhile, there are few reported studies on applying the Class E rectifiers to MHz WPT systems. Initial discussions can be found in [31], [32], where the simulation-based analysis and the real implementation of the Class E rectifiers were introduced.

Therefore, this paper is devoted to a detailed discussion on the MHz high-frequency rectification using a Class E rectifier. The analytical derivation of a Class E current-driven rectifier is given that provides guidance on the optimized parameter design of a 6.78-MHz WPT system. The current-driven topology is chosen because this topology can be used both in parallel-series (PS) and series-series (SS) WPT systems. The topology of the Class E current-driven rectifier used in this paper was first proposed in [24] for high-frequency applications. In the reference the circuit analysis was given assuming ideal devices, i.e., ideal diode and filter inductor. Based on the

Manuscript received April 19, 2015; revised July 11, 2015; accepted August 15, 2015. M. Liu, M. Fu, and C. Ma are with the University of Michigan-Shanghai Jiao Tong University Joint Institute, Shanghai Jiao Tong University, Minhang, Shanghai 200240, China (e-mail: mikeliu@sjtu.edu.cn; fuminfan@sjtu.edu.cn; chbma@sjtu.edu.cn). C. Ma is also with School of Mechanical Engineering, Shanghai Jiao Tong University, Shanghai 200240, China.

topology in [24], this paper extends its new application to MHz WPT. First an accurate input impedance of the Class E current-driven rectifier is analytically derived considering the on-resistance of the rectifying diode and the equivalent series resistance (ESR) of the filter inductor. Since the nonzero input reactance of the rectifier will detune the coupling coils from resonance, based on the derived input impedance design procedures are developed to further optimize the parameters of the 6.78-MHz WPT system including its rectifier, coupling coils, and Class E PA. Besides, analytical expressions for the component and system level efficiencies are also given, which again can guide and evaluate the design of the MHz WPT systems. In the final experiments, with loosely coupled coils (mutual inductance coefficient $k = 0.1327$) the example 6.78-MHz WPT system can still achieve a high efficiency greater than 80% over a wide range of DC loads.

This paper is organized as follows. Section II gives the circuit and performance analysis of the Class E current-driven rectifier, and analytically derives its input impedance. Based on this input impedance, section III develops procedures to design the optimal parameters for the Class E rectifier, coupling coils, and a Class E PA in a 6.78-MHz WPT system. The efficiencies of these three components and the overall WPT system are also analytically derived. Then section IV validates the analytical results by experiments using the example 6.78-MHz WPT system. Finally, section V draws the conclusions.

II. ANALYTICAL DERIVATION OF CLASS E RECTIFIER

As mentioned in the introduction, the reactance of a rectifier will detune the coupling coils from resonance. This may lower the efficiency and power transfer capability of an overall WPT system. In order to further optimize the parameter design of the system considering the influence of the rectifier, the input impedance of the Class E current-driven rectifier is analytically derived as follows.

A. Circuit Analysis

Fig. 1(a) shows the circuit of the Class E current-driven rectifier. It consists of a diode D_r , a parallel capacitor C_r , a filter capacitor C_o , a filter inductor L_r , and a DC load R_L . The idealized current and voltage waveforms of the rectifier are given in Fig. 2 that explain its principle of operation [24]. Here i_{rec} is the input current, I_o is the output DC current, i_{D_r} is the current through the diode, i_{C_r} is the current through the parallel capacitor, v_{D_r} is the diode voltage, and D is the duty cycle of the diode. As shown in Fig. 1 and Fig. 2, i_{rec} is a sinusoidal current, and the current through the filter inductor L_r equals to the DC output current I_o . Thus the parallel combination of D_r and C_r is driven by a current of $I_o + i_{rec}$. This current determines the waveforms of i_{D_r} , i_{C_r} , and v_{D_r} .

In order to analytically discuss the parameter design of the rectifier and derive its input impedance, common assumptions are usually given as follows [24][see Fig. 2]:

- 1) The rectifier is driven by a sinusoidal current source;
- 2) The forward voltage drop of the diode D_r is neglected;
- 3) The current through the filter inductor L_r is constant and equal to the output DC current I_o ;

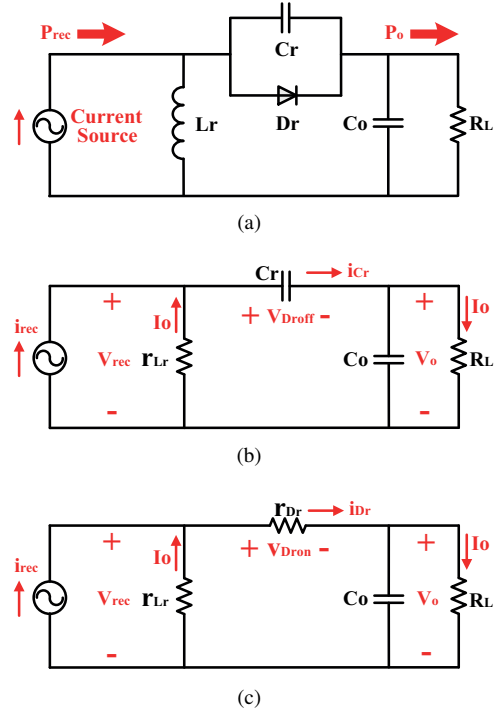


Fig. 1. The Class E current-driven rectifier. (a) Circuit model. (b) Equivalent circuit model when the diode is off. (c) Equivalent circuit model when the diode is on.

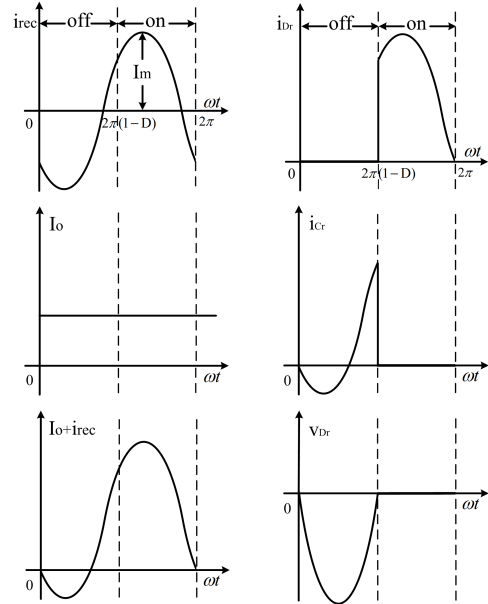


Fig. 2. Idealized current and voltage waveforms.

- 4) The output ripple voltage is sufficiently small, and thus the output voltage V_o is constant.

Suppose the input current i_{rec} is

$$i_{rec} = I_m \sin(\omega t + \phi_{rec}), \quad (1)$$

where I_m is the amplitude, ϕ_{rec} is the initial phase, and ω is the target operating frequency. When the diode is off ($0 < \omega t \leq 2\pi(1 - D)$), the rectifier can be represented using the circuit model shown in Fig. 1(b). r_{L_r} is the ESR of L_r . Thus

the current through the capacitor C_r is

$$i_{C_r} = i_{rec} + I_o = I_m \sin(\omega t + \phi_{rec}) + I_o. \quad (2)$$

As shown in Fig. 2, since i_{C_r} equals to zero when $\omega t = 0$, I_o can be determined as

$$I_o = -I_m \sin \phi_{rec}. \quad (3)$$

Hence

$$i_{C_r} = I_m [\sin(\omega t + \phi_{rec}) - \sin \phi_{rec}]. \quad (4)$$

Using (4) the voltage across the diode D_r can be derived as

$$\begin{aligned} v_{D_r,off} &= \frac{1}{\omega C_r} \int_0^{\omega t} i_{C_r} d\omega t \\ &= \frac{I_m}{\omega C_r} [\cos \phi_{rec} - \cos(\omega t + \phi_{rec}) - \omega t \sin \phi_{rec}]. \end{aligned} \quad (5)$$

When $\omega t = 2\pi(1-D)$, $v_{D_r,off}$ reaches zero. Then

$$\cos \phi_{rec} - \cos[2\pi(1-D) + \phi_{rec}] - 2\pi(1-D) \sin \phi_{rec} = 0, \quad (6)$$

and thus the relationship between ϕ_{rec} and D is obtained as

$$\tan \phi_{rec} = \frac{1 - \cos 2\pi D}{\sin 2\pi D + 2\pi(1-D)}. \quad (7)$$

Similarly the equivalent model of the rectifier is shown in Fig. 1(c) when the diode is on ($2\pi(1-D) < \omega t \leq 2\pi$). r_{D_r} is the on-resistance of diode. The current in the diode is

$$i_{D_r} = i_{rec} + I_o = I_m \sin(\omega t + \phi_{rec}) + I_o. \quad (8)$$

Since the current that flows through the diode and the capacitor is shorted out, $v_{D_r,on}$ can be represented as

$$v_{D_r,on} = [I_m \sin(\omega t + \phi_{rec}) + I_o] r_{D_r}. \quad (9)$$

Based on $v_{D_r,off}$ and $v_{D_r,on}$, the average voltage across the diode is calculated as

$$v_{D_r,avg} = \frac{1}{2\pi} \left(\int_0^{2\pi(1-D)} v_{D_r,off} d\omega t + \int_{2\pi(1-D)}^{2\pi} v_{D_r,on} d\omega t \right). \quad (10)$$

Thus substituting (5) and (9) into (10) gives

$$\begin{aligned} v_{D_r,avg} &= -\frac{I_m}{2\pi\omega C_r} \{2\pi(1-D) \cos \phi_{rec} - \sin(\phi_{rec} - 2\pi D) \\ &+ [1 - 2\pi^2(1-D)^2] \sin \phi_{rec}\} - \frac{I_m r_{D_r}}{2\pi} [(1 - \cos 2\pi D) \cos \phi_{rec} \\ &+ (2\pi D - \sin 2\pi D) \sin \phi_{rec}]. \end{aligned} \quad (11)$$

According to Fig. 1(b) and Fig. 1(c), the following relationship exists among the voltages,

$$v_{D_r,avg} + V_o + V_{L_r} = 0, \quad (12)$$

where V_o is the DC output voltage and V_{L_r} is the DC voltage drop on L_r . V_o and V_{L_r} can be given as

$$V_o = I_o R_L, \quad (13)$$

$$V_{L_r} = I_o r_{L_r}, \quad (14)$$

where I_o is the DC output current. Substituting (11), (13), and (14) into (12) yields the solution for C_r ,

$$C_r = \frac{1 + \frac{[\sin 2\pi D + 2\pi(1-D)]^2}{1 - \cos 2\pi D} - 2\pi^2(1-D)^2 - \cos 2\pi D}{2\pi\omega(R_L + r_{L_r} + r_{D_r})}. \quad (15)$$

As shown in the above equation, the duty cycle of diode, D , is determined by C_r and R_L . Under a specific R_L , D can be properly designed with C_r , i.e., the capacitance of the parallel capacitor. The design of the parameters including D and C_r will be discussed in the following section.

B. Input Impedance

Since the input current i_{rec} is sinusoidal, it is sufficient to determine the input impedance of the Class E current-drive rectifier only at the operating frequency. As shown in Fig. 3, the input impedance of the rectifier, Z_{rec} , can be represented as a series combination of the input resistance R_{rec} and the input reactance X_{rec} . Both of R_{rec} and X_{rec} are defined at the operating frequency.

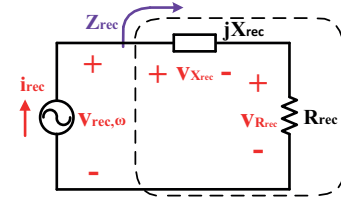


Fig. 3. Circuit model for deriving the input impedance of the Class E current-driven rectifier.

Then

$$Z_{rec} = R_{rec} + jX_{rec}. \quad (16)$$

According to KVL and Fig. 1, the input voltage of the rectifier v_{rec} is

$$v_{rec} = v_{D_r} + V_o, \quad (17)$$

where

$$v_{D_r} = \begin{cases} v_{D_r,off} & \text{when } 0 < \omega t \leq 2\pi(1-D) \\ v_{D_r,on} & \text{when } 2\pi(1-D) < \omega t \leq 2\pi. \end{cases} \quad (18)$$

The fundamental component of the input voltage, $v_{rec,\omega}$, can be expressed as

$$\begin{aligned} v_{rec,\omega} &= v_{R_{rec}} + v_{X_{rec}} \\ &= V_{m,R_{rec}} \sin(\omega t + \phi_{rec}) + V_{m,X_{rec}} \cos(\omega t + \phi_{rec}), \end{aligned} \quad (19)$$

where $V_{m,R_{rec}}$ and $V_{m,X_{rec}}$ are the amplitudes of $v_{R_{rec}}$ and $v_{X_{rec}}$, respectively. First $V_{m,X_{rec}}$ is solved through the trigonometric Fourier series for real-valued signals,

$$\begin{aligned} V_{m,X_{rec}} &= \frac{1}{\pi} \left[\int_0^{2\pi(1-D)} \cos(\omega t + \phi_{rec}) v_{D_r,off} d\omega t \right. \\ &+ \int_{2\pi(1-D)}^{2\pi} \cos(\omega t + \phi_{rec}) v_{D_r,on} d\omega t \\ &+ \left. \int_0^{2\pi} V_o \cos(\omega t + \phi_{rec}) d\omega t \right] \\ &= -\frac{I_m}{\pi} \left[\frac{a+b}{\omega C_r} + r_{D_r}(c+d) \right], \end{aligned} \quad (20)$$

where

$$a = \pi(1 - D)[1 + 2 \sin \phi_{rec} \sin(\phi_{rec} - 2\pi D)], \quad (21)$$

$$b = \sin 2\pi D + \frac{1}{4}[\sin(2\phi_{rec} - 4\pi D) - \sin 2\phi_{rec}], \quad (22)$$

$$c = \frac{1}{2} - \frac{\cos 2\phi_{rec}}{4} - \frac{\cos(2\phi_{rec} - 4\pi D)}{4}, \quad (23)$$

$$d = -\sin \phi_{rec} \sin(\phi_{rec} - 2\pi D). \quad (24)$$

Therefore, X_{rec} is

$$X_{rec} = \frac{V_{m,X_{rec}}}{I_m} = -\frac{1}{\pi} \left[\frac{a+b}{\omega C_r} + r_{D_r}(c+d) \right]. \quad (25)$$

Meanwhile, R_{rec} can be calculated based on the law of conservation of energy. The following relationship exists,

$$P_{rec} = P_o + P_{L_r} + P_{D_r}, \quad (26)$$

where P_{rec} is the input power of the rectifier, P_o is its output power, P_{L_r} is the power loss on the filter inductor L_r , and P_{D_r} is the power loss on the diode, D_r . According to Fig. 3, P_{rec} is

$$P_{rec} = \frac{I_m^2}{2} R_{rec}. \quad (27)$$

Since the current through L_r and R_L is the DC current I_o , P_o and P_{L_r} can be calculated as

$$P_o = I_o^2 R_L, \quad (28)$$

$$P_{L_r} = I_o^2 r_{L_r}, \quad (29)$$

respectively. Because the power loss on the diode only occurs at its on-state, P_{D_r} is derived as

$$P_{D_r} = \frac{1}{2\pi} \int_{2\pi(1-D)}^{2\pi} i_{D_r}^2 r_{D_r} d\omega t = e I_m^2 r_{D_r}, \quad (30)$$

where

$$e = \frac{1}{2} + \sin^2 \phi_{rec} + \frac{1}{\pi} \sin \phi_{rec} \cos(\phi_{rec} - 2\pi D) + \frac{1}{8\pi} \sin(2\phi_{rec} - 4\pi D) - \frac{9}{8\pi} \sin 2\phi_{rec}. \quad (31)$$

Substituting (27)–(30) and (3) into (26) gives

$$R_{rec} = 2\sin^2 \phi_{rec}(R_L + r_{L_r}) + 2er_{D_r}. \quad (32)$$

Then the efficiency of the Class E current-driven rectifier can be calculated as

$$\eta_{rec} = \frac{P_o}{P_{rec}} = \frac{P_o}{P_o + P_{L_r} + P_{D_r}} = \frac{R_L}{R_L + r_{L_r} + \frac{er_{D_r}}{\sin^2 \phi_{rec}}}, \quad (33)$$

and the power factor of the rectifier is

$$PF_{rec} = \frac{R_{rec}}{\sqrt{R_{rec}^2 + X_{rec}^2}}. \quad (34)$$

C. Performances

Here the performance analysis of the Class E current-driven rectifier is provided using its parasitic parameters in the following final experimental system ($r_{L_r} = 0.2 \Omega$ and $r_{D_r} = 1.4 \Omega$). The analysis includes the power output capability C_p , the ratio of the diode peak voltage to output voltage $V_{D_r,P}/V_o$, the ratio of the diode peak current to output current $I_{D_r,P}/I_o$, the ratio of output voltage to the RMS of input voltage $V_o/V_{rec,rms}$, the ratio of output current to the RMS of input current $I_o/I_{rec,rms}$, diode voltage and current waveforms, input impedance, and finally the input voltage harmonics.

For the Class E rectifier, the power output capability C_p is defined as follows,

$$C_p = \frac{P_o}{I_{D_r,P} |V_{D_r,P}|} = \frac{I_o V_o}{I_{D_r,P} |V_{D_r,P}|}, \quad (35)$$

where $V_{D_r,P}$ and $I_{D_r,P}$ are the diode peak voltage and current, respectively. According to [22] [24], the peak value of i_{D_r} occurs at $\omega t = 2\pi(1 - D)$ when $D < 0.28$. $I_{D_r,P}$ when $D \geq 0.28$ can be calculated by differentiating the diode current in (8). Thus

$$I_{D_r,P} = \begin{cases} I_o \left(1 - \frac{1}{\sin \phi_{rec}}\right) & D \geq 0.28 \\ I_o \left[1 - \frac{\sin(\phi_{rec} - 2\pi D)}{\sin \phi_{rec}}\right] & D < 0.28 \end{cases}. \quad (36)$$

Similarly, $V_{D_r,P}$ is obtained by differentiating the diode voltage in (18),

$$V_{D_r,P} = \left| \frac{V_o}{\omega C_r R_L} \{ \arcsin(\sin \phi_{rec}) - \cot \phi_{rec} - \phi_{rec} + \frac{\cos[\arcsin(\sin \phi_{rec})]}{\sin \phi_{rec}} \} \right|. \quad (37)$$

Using (35)–(37), C_p , $I_{D_r,P}/I_o$, and $V_{D_r,P}/V_o$ of the rectifier are calculated and plotted in Fig. 4 under various duty cycle D , where ϕ_{rec} is calculated from (7). For comparison purposes, the figure also includes C_p , $I_{D_r,P}/I_o$, and $V_{D_r,P}/V_o$ of the Class E voltage-driven rectifier that has been applied in a 800-kHz WPT system [28]. As shown in the figure, the Class E current-driven rectifier discussed in this paper has similar power output capacity, diode current and voltage stresses (i.e., $I_{D_r,P}/I_o$, and $V_{D_r,P}/V_o$) with the Class E voltage-driven rectifier. As mentioned in the introduction, the Class E voltage-driven rectifier can not be driven in PS and SS WPT systems; while the Class E current-driven rectifier can be used in both topologies. These two types of Class E rectifier can cover various topologies of WPT systems.

In order to investigate the performance of the rectifier under a varying load, various parameters are calculated and shown in Fig. 5 by sweeping R_L from 10Ω to 100Ω . Here the value of C_r is fixed, 237 pF, and $I_m = 1$ A. Fig. 5(a) shows that the duty cycle of the diode becomes smaller for higher load R_L and 50% duty cycle occurs when $R_L = 30 \Omega$. In Fig. 5(b)–(d), it can be seen that an increasing R_L leads to higher diode peak voltage but lower $V_{D_r,P}/V_o$ (i.e., diode voltage stress); while the diode peak current becomes lower and $I_{D_r,P}/I_o$ (i.e., diode current stress) increases. Fig. 5(e) gives the ratio of the output voltage to the RMS of input voltage and the ratio of the output current to the RMS of input

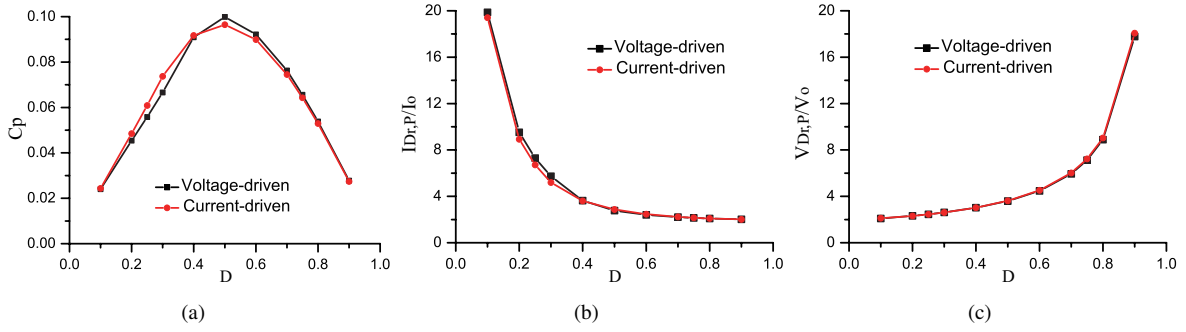


Fig. 4. Comparison with the Class E voltage-driven rectifier in [28]. (a) C_p . (b) $I_{Dr,P}/I_o$. (c) $V_{Dr,P}/V_o$.

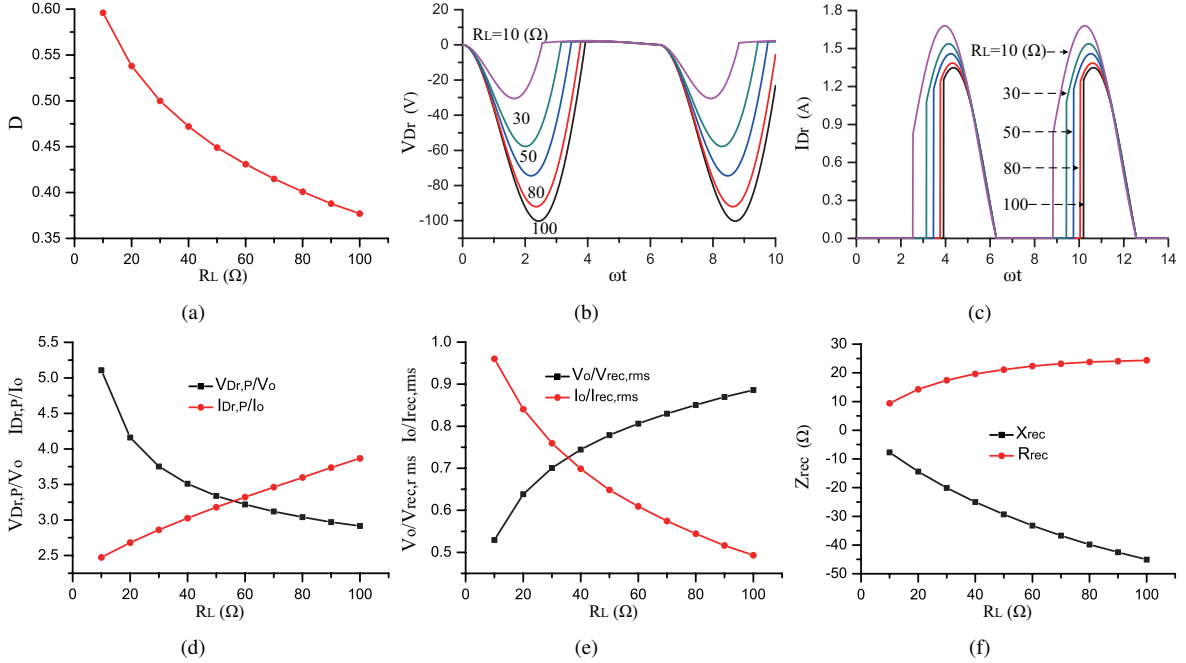


Fig. 5. Calculated values of various parameters with a varying R_L . (a) Duty cycle. (b) Waveforms of diode voltage. (c) Waveforms of diode current. (d) $V_{Dr,P}/V_o$ and $I_{Dr,P}/I_o$. (e) $V_o/V_{rec,rms}$ and $I_o/I_{rec,rms}$. (f) Input impedance.

current, which are calculated from (38) and (39), respectively. $V_o/V_{rec,rms}$ increases and $I_o/I_{rec,rms}$ decreases when R_L becomes larger. Fig. 5(f) shows that both $|X_{rec}|$ and R_{rec} increase with R_L . Since X_{rec} is negative, Z_{rec} here is a capacitive impedance. Note with fixed C_r and R_L , there is a one-to-one relationship between D and ω [24]. Thus Fig. 4 and Fig. 5(e) (D varies with R_L) also indicate the influence of the operating frequencies on the diode voltage/current stresses, and the ratio of the output voltage/current to the RMS of the input voltage/current.

$$\frac{V_o}{V_{rec,rms}} = \frac{V_o}{\sqrt{\frac{1}{2\pi} \int_0^{2\pi} v_{rec}^2 d\omega t}}. \quad (38)$$

$$\frac{I_o}{I_{rec,rms}} = \frac{\sqrt{2}I_o}{I_m}. \quad (39)$$

Finally, according to the trigonometric Fourier series formula, the N th-order harmonic content of the rectifier input

voltage can be expressed as

$$V_{m,n} = \sqrt{a_n^2 + b_n^2}, \quad (40)$$

where a_n and b_n are the Fourier coefficients,

$$a_n = \frac{1}{\pi} \left[\int_0^{2\pi(1-D)} v_{Dr,off} \cos(n\omega t + \phi_{rec}) d\omega t + \int_{2\pi(1-D)}^{2\pi} v_{Dr,on} \cos(n\omega t + \phi_{rec}) d\omega t \right]. \quad (41)$$

$$b_n = \frac{1}{\pi} \left[\int_0^{2\pi(1-D)} v_{Dr,off} \sin(n\omega t + \phi_{rec}) d\omega t + \int_{2\pi(1-D)}^{2\pi} v_{Dr,on} \sin(n\omega t + \phi_{rec}) d\omega t \right]. \quad (42)$$

The input voltage harmonic content is calculated by substituting (5)(9) into (41)(42), and shown in Fig. 6. Note here the input current of the rectifier is sinusoidal with an amplitude of 1 A.

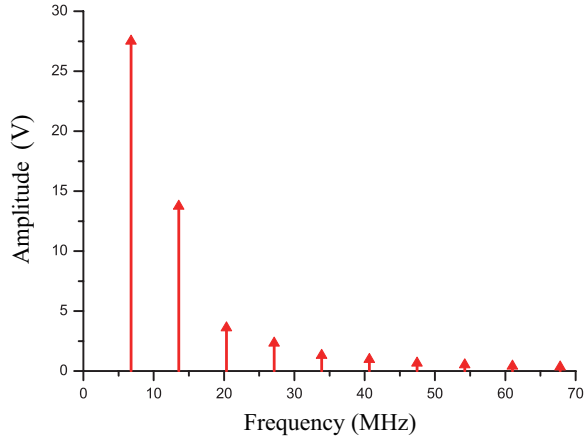


Fig. 6. The rectifier input voltage harmonics.

III. OPTIMIZED PARAMETER DESIGN

Here based on the above analytical results, the parameter design of a high-efficiency 6.78-MHz WPT system is discussed. This example WPT system consists of a power supply, a Class E PA, coupling coils, a Class E current-driven rectifier, and a final DC load, as shown in Fig. 7. In the figure, P_{rec} and P_o are the input and output power of the rectifier, respectively. P_{Zin} is the input power of coupling coils, and P_{in} is the input power of PA. Then the system efficiency is defined as

$$\eta_{sys} = \frac{P_o}{P_{in}} = \eta_{rec} \cdot \eta_{coil} \cdot \eta_{PA}. \quad (43)$$

Based on the input impedance of the Class E current-driven rectifier, the design procedures for the parameters of the three components, rectifier, coupling coils, and PA, are developed as follows.

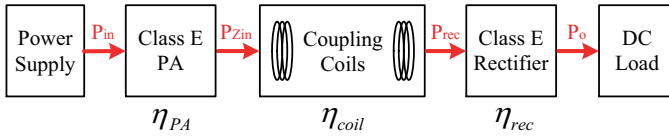


Fig. 7. Configuration of the example 6.78-MHz WPT system.

A. Rectifier

In order to minimize the voltage and current stress on the diode, the Class E rectifier is usually designed to have a 50% duty cycle for the rectifying diode [20], [24]. Thus the optimal capacitance of the parallel capacitor C_r , $C_{r,opt}$, can be determined by letting $D = 0.5$ [refer to Fig. 1 and (15)], namely

$$C_{r,opt} = \frac{747.2}{R_L + r_{L_r} + r_{D_r}} \times 10^{-12}. \quad (44)$$

As shown in the above equation, since there is a one-to-one relationship between $C_{r,opt}$ and R_L , $C_{r,opt}$ can be straightforwardly derived based on the value of R_L . Letting $D = 0.5$ in (32) gives

$$R_{rec} = 0.5768(R_L + r_{L_r}) + 0.7116r_{D_r}. \quad (45)$$

Substituting (44) into (25) yields

$$X_{rec} = -[0.6648(R_L + r_{L_r}) + 0.8484r_{D_r}]. \quad (46)$$

Thus the efficiency and power factor of the rectifier, η_{rec} and PF_{rec} , can be represented as

$$\eta_{rec} = \frac{R_L}{R_L + r_{L_r} + 1.2337r_{D_r}}, \quad (47)$$

and

$$PF_{rec} = \frac{1}{\sqrt{1 + \left[\frac{0.6648(R_L + r_{L_r}) + 0.8484r_{D_r}}{0.5768(R_L + r_{L_r}) + 0.7116r_{D_r}} \right]^2}}, \quad (48)$$

respectively.

Based on (45) and (46), the input impedance of the rectifier is plotted in Fig. 8 again using the parasitic parameters of the rectifier in final experimental system ($r_{L_r} = 0.2 \Omega$ and $r_{D_r} = 1.4 \Omega$). The figure shows that X_{rec} and R_{rec} are both the linear functions of R_L and increase with R_L when $D = 0.5$. Fig. 9 gives the efficiency and the power factor of the rectifier calculated using (47) and (48). It can be seen that η_{rec} increases with R_L , and the rectifier achieves a very high efficiency (84–98%) over a wide range of R_L ; while a relatively constant power factor is observed.

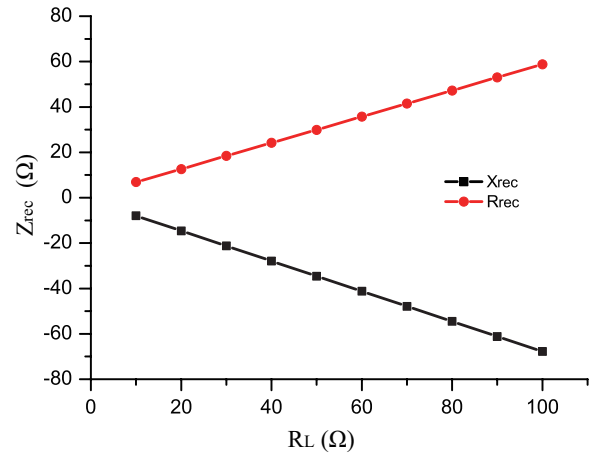


Fig. 8. Input impedance of the Class E current-driven rectifier.

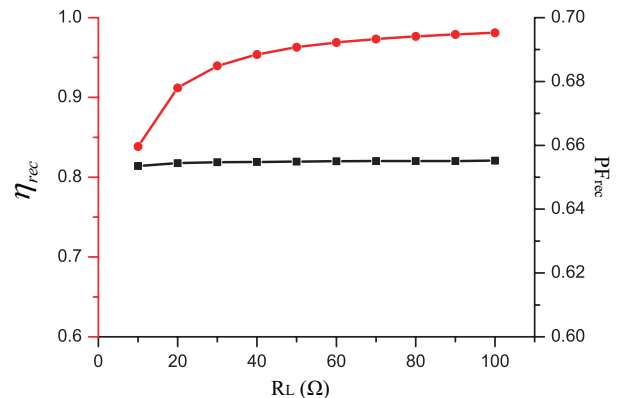


Fig. 9. Efficiency and power factor of the Class E current-driven rectifier.

B. Coupling Coils

In the conventional design the coupling coils are compensated to be resonant at a target resonance frequency, i.e., 6.78 MHz here, using an external or parasitic capacitor. Meanwhile, the influence of rectifiers is usually neglected. However, the coupling coils could be detuned from resonance due to the input reactance of a rectifier. This will lower the efficiency and power transfer capability of the coupling coils, especially when working at MHz. Using the derived input impedance of the Class E current-driven rectifier in (45) and (46), an optimal resonant capacitor can be determined that retunes the coupling coils. As shown in Fig. 10, the input impedance of the rectifier is added after the coupling coils. In the circuit, L_{tx} , r_{tx} , L_{rx} , and r_{rx} are self-inductances and self-resistances of the transmitting and receiving coils, respectively. Z_r represents the reflected impedance of the receiving coil on the transmitting side, and Z_{in} is the input impedance of the coupling coils. L_m is the mutual inductance,

$$L_m = k\sqrt{L_{tx}L_{rx}}, \quad (49)$$

where k is the mutual inductance coefficient.

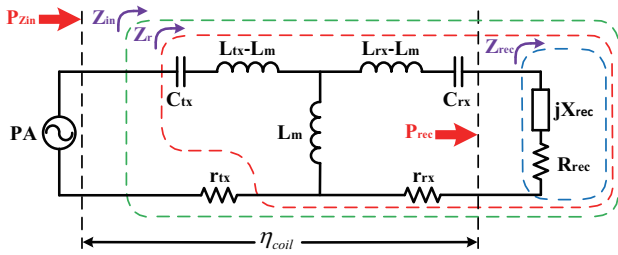


Fig. 10. Circuit model of the coupling coils.

Due to the existence of X_{rec} , C_{tx} and C_{rx} should be designed following the below equations in order to make the two coils resonant,

$$j\omega L_{rx} + \frac{1}{j\omega C_{rx}} + jX_{rec} = 0, \quad (50)$$

$$j\omega L_{tx} + \frac{1}{j\omega C_{tx}} = 0, \quad (51)$$

where ω is the target resonant frequency, 6.78 MHz here. Therefore,

$$C_{rx} = \frac{1}{\omega(\omega L_{rx} + X_{rec})}. \quad (52)$$

Substituting (46) into (52) gives the optimal $C_{rx,opt}$,

$$C_{rx,opt} = \frac{1}{\omega[\omega L_{rx} - (0.6648(R_L + r_{L_r}) + 0.8484r_{D_r})]}. \quad (53)$$

Based on Fig. 10 and under the conditions of (50) and (51), Z_r is derived as

$$Z_r = \frac{\omega^2 k^2 L_{tx} L_{rx}}{r_{rx} + R_{rec}}. \quad (54)$$

After substituting (45) into (54), the input impedance Z_{in} can be calculated,

$$Z_{in} = r_{tx} + Z_r = r_{tx} + \frac{\omega^2 k^2 L_{tx} L_{rx}}{r_{rx} + 0.5768(R_L + r_{L_r}) + 0.7116r_{D_r}}. \quad (55)$$

As shown in the above equation, the input impedance Z_{in} is pure resistive because its reactance is fully compensated by $C_{rx,opt}$ on the receiving side. And this compensation does not depend on the relative position of the coupling coils (i.e., k) [refer to (53)]. Here the efficiency of the coupling coils is defined as

$$\eta_{coil} = \frac{P_{rec}}{P_{Z_{in}}}, \quad (56)$$

where $P_{Z_{in}}$ is the input power of the transmitting coil and P_{rec} is the input power of the rectifier. For the coupling coils, the power losses only occur on r_{tx} and r_{rx} . Thus η_{coil} can also be represented as

$$\eta_{coil} = \frac{\text{Re}\{Z_r\}}{r_{tx} + \text{Re}\{Z_r\}} \cdot \frac{\text{Re}\{Z_{rec}\}}{r_{rx} + \text{Re}\{Z_{rec}\}}, \quad (57)$$

where $\text{Re}\{*\}$ means the real part of a complex number. Then substituting (45) and (54) into (57) gives the efficiency of the coupling coils,

$$\eta_{coil} = \frac{\omega^2 L_m^2 [0.5768(R_L + r_{L_r}) + 0.7116r_{D_r}]}{r_{rx} + 0.5768(R_L + r_{L_r}) + 0.7116r_{D_r} + \omega^2 L_m^2}. \quad (58)$$

This efficiency is a function of R_L and k according to (49) and (58). It is different with the efficiencies given in the previous papers, in which the efficiency was represented using an equivalent AC load [7]–[9], [11]. The existing representations of the efficiency of coupling coils are inaccurate in real applications due to their neglected input reactances of the rectifiers.

C. Power Amplifier

In the example 6.78-MHz WPT system a Class E PA is used to drive the coupling coils. Its equivalent circuit is shown in Fig 11. The PA consists of a DC power supply V_{dc} , a RF choke L_f , a switch S , a shunt capacitor C_s , a series capacitor C_0 , and a series inductor L_0 . The series L_0 - C_0 can be represented as a pure reactance X_0 . Z_{in} is the input impedance of the coupling coils. P_{in} is the input power of the PA and $P_{Z_{in}}$ is the input power of the coupling coils. Then the efficiency of PA can be defined as

$$\eta_{PA} = \frac{P_{Z_{in}}}{P_{in}}. \quad (59)$$

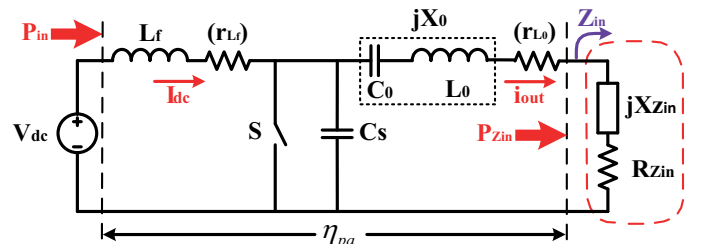


Fig. 11. Circuit model of the Class E PA.

Under the conditions of a 50% duty cycle of S and neglected parasitic parameters of the PA, the following equations, (60)–(67), were used to calculate the efficiency of the PA [33],

$$P_{in} = I_{dc}^2 R_{dc}, \quad (60)$$

$$P_{Z_{in}} = \frac{i_{out}^2 R_{Z_{in}}}{2}, \quad (61)$$

$$i_{out} = g I_{dc} = g \frac{V_{dc}}{R_{dc}}, \quad (62)$$

$$R_{dc} = \frac{\pi^2 - g(2\pi \cos \phi + 4 \sin \phi)}{4\pi\omega C_S}, \quad (63)$$

$$(64)$$

and

$$g = \frac{2\pi \sin(\varphi + \phi) + 4\cos(\varphi + \phi)}{4 \cos \phi \sin(\varphi + \phi) + \pi \cos \varphi}, \quad (65)$$

$$\varphi = \arctan \frac{X_0}{R_{Z_{in}}}, \quad (66)$$

$$\phi = \arctan \frac{\frac{\pi^2}{2} - 4 - \pi\omega C_S(2R_{Z_{in}} + \pi X_0)}{\pi + \pi^2\omega C_S R_{Z_{in}} - 2\pi\omega C_S X_0}, \quad (67)$$

where g and φ are the intermediate variables, I_{dc} is the DC input current of PA, i_{out} is the output current of PA, ϕ is initial phase of i_{out} , and R_{dc} is the equivalent resistance PA shows to the DC power supply. In order to achieve zero-voltage switching (ZVS) and maximize the PA efficiency, it is known that (68) and (69) can be used to determine C_S and X_0 [33],

$$C_S = \frac{0.1836}{\omega R_{Z_{in}}}, \quad (68)$$

$$X_0 = 1.1525 R_{Z_{in}}. \quad (69)$$

Substituting (55) into (68) and (69) yields the optimal parameters for PA,

$$C_{S,opt} = \frac{0.1836[r_{rx} + 0.5768(R_L + r_{L_r}) + 0.7116r_{D_r}]}{\omega r_{tx}[r_{rx} + 0.5768(R_L + r_{L_r}) + 0.7116r_{D_r}] + \omega^3 L^2 m}. \quad (70)$$

$$X_{0,opt} = 1.1525 r_{tx} + \frac{1.1525 \omega^2 k^2 L_{tx} L_{rx}}{r_{rx} + 0.5768(R_L + r_{L_r}) + 0.7116r_{D_r}}. \quad (71)$$

Note the pure resistive impedance Z_{in} in (55) equals with $R_{Z_{in}}$ here. Again $C_{S,opt}$ and $X_{0,opt}$ are determined by R_L and k .

In the above efficiency calculation, (60)–(67), the ESRs r_{L_f} and r_{L_0} are not included. Here r_{L_f} is the ESR of L_f and r_{L_0} is the ESR of L_0 . In order to have a more accurate calculation of the efficiency, in this paper the power losses on r_{L_f} and r_{L_0} are taken into account. Thus the modified input power P'_{in} is

$$P'_{in} = P_{in} + P_{L_0} + P_{L_f}, \quad (72)$$

where P_{in} is calculated using (60), P_{L_f} is the power loss on r_{L_f} , and P_{L_0} is the power loss on r_{L_0} . As shown in Fig. 11, P_{L_f} and P_{L_0} can be derived as

$$P_{L_f} = I_{dc}^2 r_{L_f}, \quad (73)$$

$$P_{L_0} = \frac{i_{out}^2 r_{L_0}}{2} = \frac{(g I_{dc})^2 r_{L_0}}{2}. \quad (74)$$

Then P'_{in} and η_{PA} can be calculated as

$$P'_{in} = \frac{V_{dc}^2}{R_{dc}} + \frac{V_{dc}^2}{R_{dc}^2} r_{L_f} + \frac{V_{dc}^2}{2R_{dc}^2} g^2 r_{L_0}, \quad (75)$$

and

$$\eta_{PA} = \frac{P_{Z_{in}}}{P'_{in}} = \frac{g^2 R_{Z_{in}}}{2R_{dc} + 2r_{L_f} + g^2 r_{L_0}}, \quad (76)$$

respectively.

IV. EXPERIMENTAL VERIFICATION

A 6.78-MHz WPT system is built up to verify the results of the above analytical derivations and parameter design. Its power level is up to 30 W. As shown in Figs. 12 and 13, this experimental WPT system includes a Class E PA, coupling coils, a Class E current-driven rectifier, and an electronic load. The PA, coupling coils, and the rectifier were all designed and fabricated in house. The ESR of the inductors and the on-resistance of diode are also labeled in Fig. 13. In this 6.78-MHz WPT system the rectifying diode D_r is a Schottky silicon carbide diode (STPSC406) and a MOSFET (SUD06N10) works as the switch S . Their parasitic capacitors are about 25 pF and 40 pF, respectively. Here the diode D_r operates at a peak voltage around 100 V and a power level of 20 W. Therefore its parasitic capacitance is assumed to be constant, 25 pF, according to the datasheet.

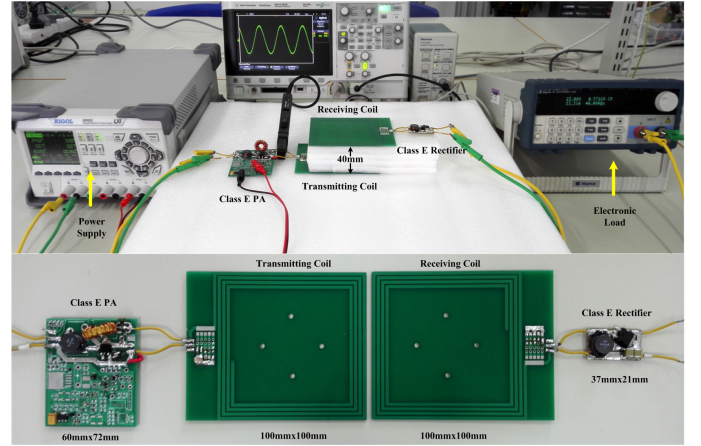


Fig. 12. The experimental 6.78-MHz WPT system.

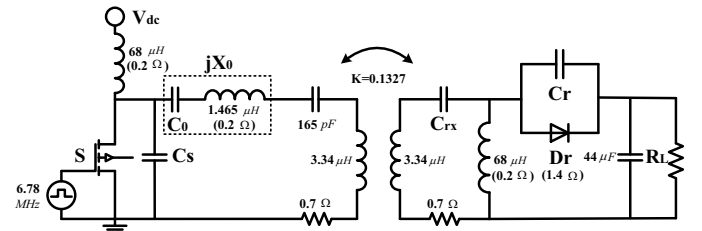


Fig. 13. The circuit and parameters of the experimental system.

As discussed above, C_r , C_{rx} , C_S , and X_0 are the design parameters of the WPT system. Their optimal values are

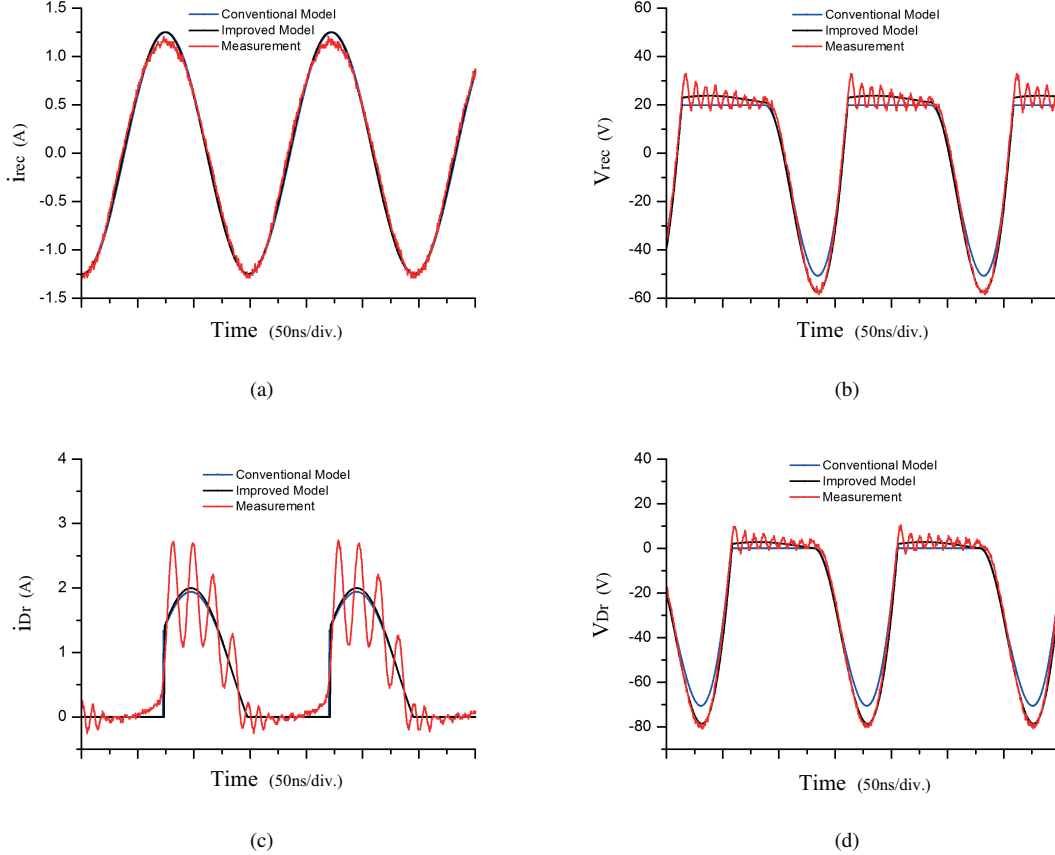


Fig. 14. Measured and calculated waveforms of the Class E current-driven rectifier. (a) Input current. (b) Input voltage. (c) Diode current. (d) Diode voltage.

calculated using (44), (53), (70), and (71), and listed in Table I under various R_L . The PA series capacitor, C_0 , is then determined by X_0 . Note the parasitic capacitances of D_r and S are included in the calculation. In the experiments waveforms are measured using the voltage and current probes of the oscilloscope. In order to minimize the impact of the probes, the measurements of voltage and current are not carried out at the same time. For example, the voltage probe is disconnected from the rectifier before the current measurement. Since the pin of the diode is short, the length of the pin is extended using an additional wire for the diode current measurement. Note this wire is removed in other measurements.

TABLE I
THE OPTIMAL DESIGN PARAMETERS

R_L (Ω)	C_r (pF)	C_{rx} (pF)	C_S (pF)	X_0 (Ω)
10	644	175	90	55
20	346	184	157	32
30	237	194	223	22
40	180	205	287	17
50	145	218	350	14
60	121	232	411	12
70	104	249	471	11
80	92	267	530	9.4
90	82	289	588	8.5
100	74	315	634	7.7

A. Class E Current-Driven Rectifier

Fig. 14–16 show the measured and calculated results of the Class E rectifier taking the case of $R_L = 30 \Omega$ and $C_r = 237$ pF as an example [refer to Table I]. For comparison purposes, the results using both the improved and conventional models of the rectifier are shown [24]. Besides, the actual behaviors of the rectifier were tested and measured in the experimental WPT system. Fig. 14(a) shows that the measured input current of the rectifier, i_{rec} , is sinusoidal that matches the assumption 1) in section II-A. Based on the sinusoidal input currents in Fig. 14(a), the diode currents of the two models are calculated and given in Fig. 14(c). The measured value is also included. The oscillations in the measured diode current are due to the lead inductances of the additional wire when using the current probe. In the input voltage and diode voltage waveforms, Fig. 14(b)(d), the improved model shows better accuracy thanks to the included ESR of the inductor L_r and on-resistance of the diode D_r . As shown in these figures, the voltage and current waveforms are typical waveforms for the Class E current-driven rectifier [see Fig. 2]. Fig. 15 gives the results of the diode peak voltage versus the peak to peak value of i_{rec} . Here the peak to peak value of i_{rec} is tuned by adjusting the PA DC input voltage V_{dc} [see Fig. 13]. It can be seen that the diode peak voltage is proportional to the peak to peak value of i_{rec} , and again the calculated result using the improved model is more accurate than that using the

conventional model. The maximum improvement in accuracy is about 7%. Fig. 16 shows the output voltage (V_o) and output current (I_o) of the rectifier versus the peak to peak value of i_{rec} . Again V_o and I_o both increase linearly when the peak to peak value of i_{rec} is swept from 1 A to 3 A. Similarly, the calculated results of V_o and I_o using the improved model are more accurate.

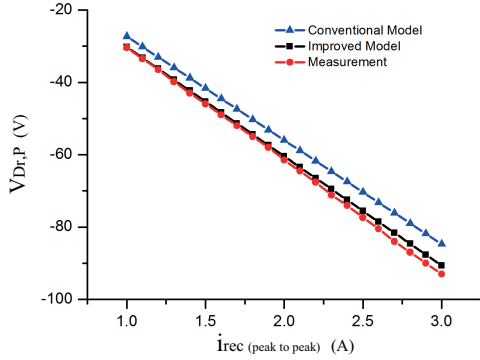


Fig. 15. Diode peak voltage versus the peak to peak value of the rectifier input current.

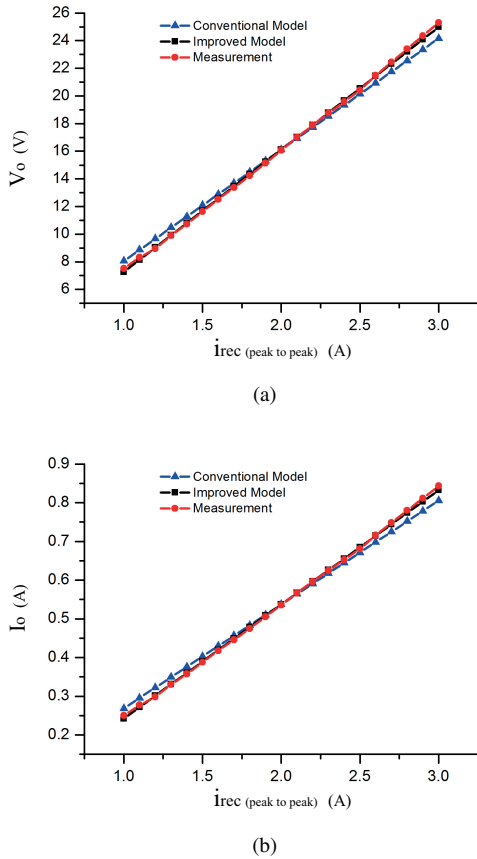


Fig. 16. Rectifier output voltage and output current versus the peak to peak value of the rectifier input current. (a) Output voltage. (b) Output current.

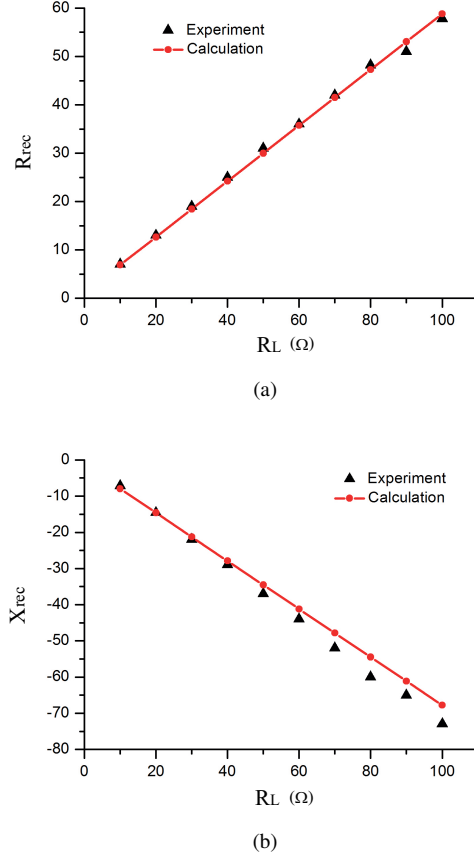


Fig. 17. Input impedance of the Class E current-driven rectifier. (a) Resistance. (b) Reactance.

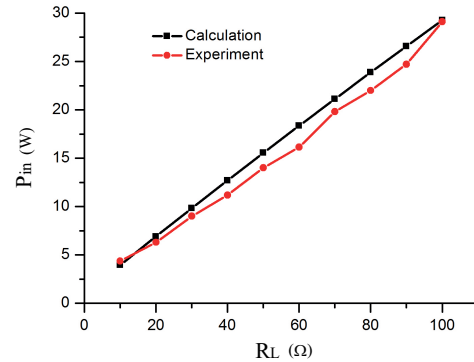


Fig. 18. Input power of PA with a fixed V_{dc} (=18 V).

B. Parameter Design of WPT System

In this paper the input impedance of the Class E current-driven rectifier is derived and guides the system-level design of MHz WPT systems. Based on the optimal design parameters given in Table I, the analytically derived input impedance of the Class E current-driven rectifier (i.e., Z_{rec}) is verified by experiments. With the 50% duty cycle of the diode D_r , the measured values of X_{rec} and R_{rec} are shown and compared with their calculated values in Fig. 17 (here C_r , C_{rx} , C_s , and X_0 vary with R_L , as listed in Table I). The measured

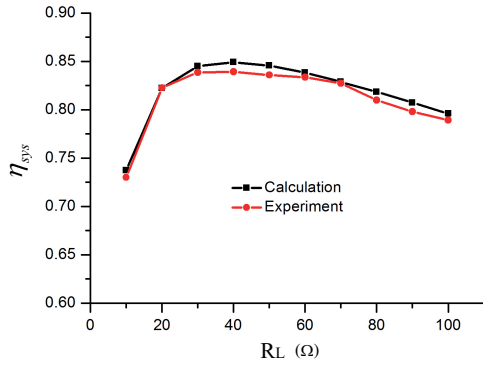


Fig. 19. System efficiency under a power level of 20 W.

data is obtained through the fast Fourier transform (FFT) of the raw data from the oscilloscope. It can be seen that the calculated and measured values well match each other. This good matching validates the correctness of the analytic representation of Z_{rec} in (25) and (32).

Fig. 18 shows the calculated and measured input power of PA under the optimal parameters in Table I and a fixed DC input voltage V_{dc} (=18 V) [refer to (75) and Fig. 13]. Again there is a good matching between the calculated and measured values over a wide range of R_L . Bigger R_L , smaller $R_{Z_{in}}$, and thus larger the input power of PA [refer to Fig. 11 and (55)]. Fig. 19 compares the system efficiencies, η_{sys} 's, under a same power level of 20 W [refer to (43)]. With the optimal parameters, the 6.78-MHz WPT system achieves a high DC to DC efficiency over a wide range of R_L both in the calculation and experimental results. The highest efficiency reaches about 84% even here the coils are loosely coupled, i.e., $k=0.1327$ in Fig. 13. Again the good matching between the two results verifies that the above analytical results are sufficiently accurate to guide the design of a real WPT system.

V. CONCLUSIONS

This paper discusses optimized parameter design of a 6.78-MHz WPT system based on the analytical derivation of the Class E current-driven rectifier. The input impedance of the Class E rectifier is accurately derived considering the on-resistance of the diode and the ESR of the filter inductor. Then this derived input impedance is used to guide the parameter design of the rectifier, coupling coils, and the Class E PA. Furthermore, both the component and system level efficiencies are also analytically derived. The analytical results are found to well match the experimental results. With loosely coupled coils, high system efficiencies greater than 80% are achieved over a wide range of DC loads in the final experiments. Possible future directions of this work may include the extension of the analysis to the Class E full-wave rectifiers and investigate their cost performances in real WPT applications.

REFERENCES

[1] A. P. Hu, *Wireless/Contactless Power Supply: Inductively coupled resonant converter solutions*. Saarbrücken, Germany: VDM Publishing, 2009.

[2] C.-S. Wang, O. H. Stielau, and G. A. Covic, "Design considerations for a contactless electric vehicle battery charger," *IEEE Trans. Ind. Electron.*, vol. 52, no. 5, pp. 1308–1314, 2005.

[3] N. Shinohara, "Power without wires," *IEEE Microw. Magazine*, vol. 12, no. 7, pp. S64–S73, 2011.

[4] J. T. Howell, M. J. O'Neill, and R. L. Fork, "Advanced receiver/converter experiments for laser wireless power transmission," in *Proc. The 4th International Conference on Solar Power from Space (SPS04)*, vol. 567, Granada, Spain, 30 June–2 July 2004, pp. 187–194.

[5] A. Kurs, A. Karalis, R. Moffatt, J. D. Joannopoulos, P. Fisher, and M. Soljačić, "Wireless power transfer via strongly coupled magnetic resonances," *science*, vol. 317, no. 5834, pp. 83–86, 2007.

[6] S. Hui, W. Zhong, and C. Lee, "A critical review of recent progress in mid-range wireless power transfer," *IEEE Trans. Power Electron.*, vol. 29, no. 9, pp. 4500–4511, Sept 2014.

[7] W. Zhong, C. Zhang, X. Liu, and S. Hui, "A methodology for making a three-coil wireless power transfer system more energy efficient than a two-coil counterpart for extended transfer distance," *IEEE Trans. Power Electron.*, vol. 30, no. 2, pp. 933–942, Feb 2015.

[8] M. Fu, T. Zhang, C. Ma, and X. Zhu, "Efficiency and optimal loads analysis for multiple-receiver wireless power transfer systems," *IEEE Trans. Microw. Theory Tech.*, vol. 63, no. 3, pp. 801–812, 2015.

[9] M. Pinuela, D. C. Yates, S. Lucyszyn, and P. D. Mitcheson, "Maximizing DC-to-load efficiency for inductive power transfer," *IEEE Trans. Power Electron.*, vol. 28, no. 5, pp. 2437–2447, 2013.

[10] A. Sample, B. Waters, S. Wisdom, and J. Smith, "Enabling seamless wireless power delivery in dynamic environments," *Proc. IEEE*, vol. 101, no. 6, pp. 1343–1358, June 2013.

[11] S.-H. Lee and R. D. Lorenz, "Development and validation of model for 95%-efficiency 220-w wireless power transfer over a 30-cm air gap," *IEEE Trans. Appl. Ind.*, vol. 47, no. 6, pp. 2495–2504, 2011.

[12] S. Aldhaher, P.-K. Luk, and J. F. Whidborne, "Electronic tuning of misaligned coils in wireless power transfer systems," *IEEE Trans. Power Electron.*, vol. 29, no. 11, pp. 5975–5982, 2014.

[13] S. Aldhaher, P.-K. Luk, A. Bati, and J. Whidborne, "Wireless power transfer using Class E inverter with saturable DC-feed inductor," *IEEE Trans. Ind. Appl.*, vol. 50, no. 4, pp. 2710–2718, July 2014.

[14] P. Srimuang, N. Puangngernmak, and S. Chalermwisutkul, "13.56 MHz Class E power amplifier with 94.6% efficiency and 31 watts output power for RF heating applications," in *Electrical Engineering/Electronics, Computer, Telecommunications and Information Technology (ECTI-CON), 11th International Conference on*. IEEE, 2014, pp. 1–5.

[15] T. Suetsugu and M. Kazimierczuk, "Analysis and design of Class E amplifier with shunt capacitance composed of nonlinear and linear capacitances," *IEEE Trans. Circuits Syst.*, vol. 51, no. 7, pp. 1261–1268, July 2004.

[16] M. Fu, H. Yin, X. Zhu, and C. Ma, "Analysis and tracking of optimal load in wireless power transfer systems," *Power Electronics, IEEE Transactions on*, vol. 30, no. 7, pp. 3952–3963, July 2015.

[17] M. Fu, C. Ma, and X. Zhu, "A cascaded boost-buck converter for high efficiency wireless power transfer systems," *IEEE Trans. Ind. Informat.*, vol. 10, no. 3, pp. 1972–1980, 2014.

[18] T. Zhang, M. Fu, C. Ma, and X. Zhu, "Optimal load analysis for a two-receiver wireless power transfer system," in *Wireless Power Transfer Conference (WPTC)*. IEEE, 2014, pp. 84–87.

[19] M. Kazimierczuk and J. Jozwik, "Class-E zero-voltage-switching and zero-current-switching rectifiers," *IEEE Trans. Circuits Syst.*, vol. 37, no. 3, pp. 436–444, Mar 1990.

[20] S. Birca-Galateanu and A. Ivascu, "Class E low dv/dt and low di/dt rectifiers: energy transfer, comparison, compact relationships," *IEEE Trans. Circuits Syst. I, Fundam. Theory Appl.*, vol. 48, no. 9, pp. 1065–1074, Sep 2001.

[21] W. Nitz, W. Bowman, F. Dickens, F. Magalhaes, W. Strauss, W. Suiter, and N. Ziesse, "A new family of resonant rectifier circuits for high frequency DC-DC converter applications," in *Proc. Appl., Power Electron. Conf.*, Feb 1988, pp. 12–22.

[22] A. Ivascu, M. Kazimierczuk, and S. Birca-Galateanu, "Class E resonant low dv/dt rectifier," *IEEE Trans. Circuits Syst. I, Fundam. Theory Appl.*, vol. 39, no. 8, pp. 604–613, Aug 1992.

[23] M. Kazimierczuk and W. Szaraniec, "Analysis of a Class E rectifier with a series capacitor," *Circuits, Devices and Systems, IEE Proceedings G*, vol. 139, no. 3, pp. 269–276, Jun 1992.

[24] M. Kazimierczuk, "Class E low dv/dt rectifier," *IEEE Trans. Power Electron.*, vol. 136, no. 6, pp. 257–262, Nov 1989.

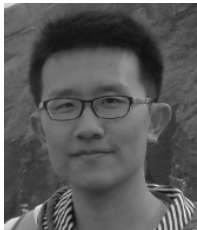
- [25] J. Jozwik and M. Kazimierczuk, "Analysis and design of Class- E^2 DC/DC converter," *IEEE Trans. Ind. Electron.*, vol. 37, no. 2, pp. 173–183, Apr 1990.
- [26] Y. Minami and H. Koizumi, "Analysis of Class DE current driven low d_i/d_t rectifier," *IEEE Trans. on Power Electron.*, vol. 30, no. 12, pp. 6804–6816, Dec. 2015.
- [27] A. Reatti, M. Kazimierczuk, and R. Redl, "Class E full-wave low dv/dt rectifier," *IEEE Trans. Circuits Syst. I, Fundam. Theory Appl.*, vol. 40, no. 2, pp. 73–85, Feb 1993.
- [28] S. Aldhafer, P.-K. Luk, K. El Khamlichi Drissi, and J. Whidborne, "High-input-voltage high-frequency Class E rectifiers for resonant inductive links," *IEEE Trans. Power Electron.*, vol. 30, no. 3, pp. 1328–1335, March 2015.
- [29] P.-K. Luk, S. Aldhafer, W. Fei, and J. Whidborne, "State-space modeling of a Class E^2 converter for inductive links," *IEEE Trans. Power Electron.*, vol. 30, no. 6, pp. 3242–3251, June 2015.
- [30] T. Nagashima, K. Inoue, X. Wei, E. Bou, E. Alarcon, and H. Sekiya, "Inductively coupled wireless power transfer with Class- E^2 DC-DC converter," in *Circuit Theory and Design (ECCTD), 2013 European Conference on*, Sept 2013, pp. 1–4.
- [31] T. Nagashima, X. Wei, and H. Sekiya, "Analytical design procedure for resonant inductively coupled wireless power transfer system with Class-DE inverter and Class-E rectifier," in *Circuits and Systems (APCCAS), Asia Pacific Conference on*. IEEE, Nov 2014, pp. 288–291.
- [32] G. Kkelis, J. Lawson, D. Yates, M. Pinuela, and P. Mitcheson, "Integration of a Class-E low dv/dt rectifier in a wireless power transfer system," in *Proc. Wireless Power Transfer Conf.*, May 2014, pp. 72–75.
- [33] M. Albulut, *RF power amplifiers*. SciTech Publishing, 2001.



Ming Liu (S'15) received the B.S. degree from SiChuan University, Sichuan, China, in 2007, and the M.S. degree from University of Science and Technology Beijing, Beijing, China, in 2011, both in mechatronic engineering. He is currently working toward the Ph.D. degree in electrical and computer engineering, University of Michigan-Shanghai Jiao Tong University Joint Institute, Shanghai Jiao Tong University, Shanghai, China.

His research interests include component- and system-level design of megahertz wireless power

transfer systems.



Minfan Fu (S'13) received the B.S. and M.S. degrees both in electrical and computer engineering from the University of Michigan-Shanghai Jiao Tong University Joint Institute, Shanghai Jiao Tong University, Shanghai, China, in 2010 and 2013, respectively, where he is currently working toward the Ph.D. degree.

His research interests include power electronics, control, and their applications in wireless power transfer.



Chengbin Ma (M'05) received the B.S.E.E. (Hons.) degree from East China University of Science and Technology, Shanghai, China, in 1997, and the M.S. and Ph.D. degrees both in the electrical engineering from University of Tokyo, Tokyo, Japan, in 2001 and 2004, respectively.

He is currently an assistant professor of electrical and computer engineering with the University of Michigan-Shanghai Jiao Tong University Joint Institute, Shanghai Jiao Tong University, Shanghai, China. Between 2006 and 2008, he held a post-

doctoral position with the Department of Mechanical and Aeronautical Engineering, University of California Davis, California, USA. From 2004 to 2006, he was a R&D researcher with Servo Laboratory, Fanuc Limited, Yamanashi, Japan. His research interests include wireless power transfer, networked hybrid energy system, electric vehicle, and mechatronic control.